JOURNAL OF SOLID STATE CHEMISTRY 64, 1–21 (1986)

Nonstoichiometric Forms of Sb_2S_3 Occurring in the $PbSb_2S_4$–Sb_2S_3 Region of the Pb–Sb–S Phase Diagram

R. J. D. TILLEY[1] AND A. C. WRIGHT[2]

School of Materials Science, University of Bradford, Bradford, West Yorkshire, BD7 1DP, Great Britain

Received July 26, 1985; in revised form November 18, 1985

The Sb_2S_3–PbS phase diagram suggests that Sb_2S_3 is not able to incorporate PbS into its structure to form nonstoichiometric compounds. This has been verified when Sb_2S_3 is reacted with PbS at 748 K. However, in samples which were melted and then cooled, powder X-ray diffraction showed that a nonstoichiometric form of Sb_2S_3 was produced in the composition range between Sb_2S_3 and the eutectic point at approximately 77 mole% Sb_2S_3 : 23 mole% PbS. Transmission electron microscopy showed that three defect types accounted for this nonstoichiometric region. These were (i) at lowest PbS concentrations, clusters of new structure coherently intergrown within the Sb_2S_3 crystals; (ii) at about 15 mole% PbS lamellae of a new structure coherently intergrown with the Sb_2S_3 matrix along (101) planes; (iii) at the highest PbS concentrations, near to 20 mole% planar faults on (100) planes of the Sb_2S_3 structure. Beyond the eutectic point X-ray diffraction showed that only ordered material formed.

Introduction

The increasing use of electron microscopy to study the microstructures of nonstoichiometric compounds has revealed that point defects are by no means the only way of accommodating changes in nonmetal-to-metal ratio structurally. These results have had a wide bearing on crystal chemistry and have lead to considerable revision of theoretical models to account for the formation and stability of nonstoichiometric compounds. In addition, the results are also of relevance to applied research, as many nonstoichiometric materials are of use as electronic components, as catalysts, and lately in applications involving integrated optical engineering.

The experimental data so far assembled relates mainly to oxides, and in particular to a group of oxides which form crystallographic shear structures as their stoichiometry is varied. In order to broaden the base of experimental results, it is important to study as many other nonstoichiometric phases as possible. One family which lends itself to such a study is the so-called sulfosalt group of compounds. These are principally compounds formed between PbS and the group V sulfides of As, Sb, and Bi.

The sulfosalts are widespread in nature, and although usually found as accessory

[1] Present address: Dept. of Metallurgy and Materials Science, University College, Newport Road, Cardiff CF2 1TA, G.B.

[2] Present address: Dept. of Chemistry, Solid State Chemistry Group, UMIST, P.O. Box 88, Manchester M60 1QD, G.B.

0022-4596/86 $3.00

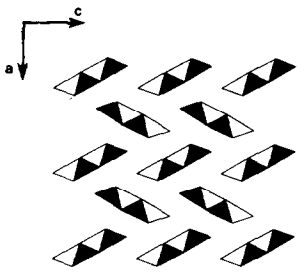

FIG. 1. Schematic depiction of the structure of Sb_2S_3 projected onto (010). The structure is composed of infinitely long ribbons, four half octahedra wide shown as black or white triangles, in this projection. The ribbons outline the positions of the sulfur atoms; the metal atoms are not shown.

minerals, they are of considerable interest to mineralogists as geological indicators. Thus phase diagram data is available which shows that a large number of complex phases form in these systems, many of which would appear to be ideal for study by electron microscopy. In order to clarify detail as much as possible, we have chosen to work with synthetic compounds prepared from high-purity chemicals rather than to examine minerals. Part of these studies, on some aspects of the PbS–Bi_2S_3 and PbS–Sb_2S_3 systems, have already been published (*1–3*). The present paper reports on a high-resolution electron microscope study of the Sb_2S_3-rich region of the PbS–Sb_2S_3 system. Despite the fact that previously published phase diagrams indicated that this part of the composition range contained no non-stoichiometric compounds, a number of new structures have been found, and new methods of accommodating changes in the anion to cation ratio in nonstoichiometric Sb_2S_3 have been discovered and presented in this paper.

Previous Studies

The system Sb–S was examined by Hansen and Anderko (*4*) who found only one stable phase, of composition Sb_2S_3, which melted congruently at 844 K and appeared to exhibit no composition range. The structure of Sb_2S_3 has been refined by Bayliss and Nowacki (*5*) and is shown in Fig. 1. It is orthorhombic, with a = 1.13107 nm, b = 0.3836 nm, c = 1.12285 nm and is isomorphous with Bi_2S_3 (*6*). The structure can be described as made up of infinite ribbons of four square pyramids, running parallel to the b axis. The square pyramids can be formally converted to octahedra if the lone-pair electrons associated with the Sb atoms are considered, for packing purposes, as anions in the manner described by Andersson and Åström (*7*). An alternative way of describing the structure in terms of trigonal prismatic coordination has also been utilized (*8*). Only one previous electron microscope study has been made on Sb_2S_3 (*9*). This involved examination of thin evaporated films of Sb_2S_3 and so is not of direct relevance to the present work on massive crystals. However, it can be noted that a variety of defects were found, but as the study was at low resolution, their structures were not determined.

All previous studies of the Sb_2S_3-rich half of the PbS–Sb_2S_3 system report only a simple eutectic occurring at approximately 22 mole% PbS with a eutectic temperature close to 818 K. The only phases found were Sb_2S_3 itself and $PbSb_2S_4$, which corresponds to the mineral zinckenite. The structure of the phase zinckenite has been determined by Portheine and Nowacki (*10*) as hexagonal with a = 2.2148 nm and c = 0.4333 nm.

Previous work on phase relations, particularly with respect to the composition range of Sb_2S_3, is not altogether of one mind. A study by Craig *et al.* (*11*) showed Sb_2S_3 not to exhibit any solid solution range towards PbS. Its melting point was found to be 853 ± 3 K. These results are very similar to those of Garvin (*12*) except that Sb_2S_3 was found to melt at 848 K. In contrast to these studies, Salanci and Moh (*13*) re-

ported that Sb_2S_3 had a composition range. Sb_2S_3 was found to show a maximum solubility of PbS of 1.5 mole% at the eutectic temperature of 819 ± 3 K. The melting point of Sb_2S_3 was found to be 856 ± 3 K. A more recent study by Salanci (*14*) introduced no new information for this region of the PbS–Sb_2S_3 system. The melting point of Sb_2S_3 was found to be 857 ± 5 K.

Experimental

All samples were prepared from "Specpure" grade lead, antimony, and sulfur supplied by Johnson Matthey Ltd. The sulfur was used as supplied, but both the lead and antimony had a tendency to tarnish in air and fresh material was prepared when new samples were required. For lead this involved paring shavings from the interior of a lead rod with a clean surgical scalpel. For antimony, as-supplied lumps were crushed in a clean percussion mortar and nonsurface fragments were selected for use in sample preparations.

Reactions were carried out by heating a total weight of 3 g of material in sealed evacuated silica tubes. In order to control the sample temperature accurately the sealed tubes were placed into holes drilled in a nickel alloy cylinder which served both as an effective high thermal mass enclosure and also protected the tubes from direct radiation from the heating elements. By using a pair of thermocouples in contact with the metal cylinder, sample temperatures could be set to within ±2 K. During reaction, temperature variation did not exceed ±5 K.

Three series of samples were prepared between the compositions Sb_2S_3 and approximately $PbSb_2S_4$. The first of these used the elements Pb, Sb, and S as the starting materials. The samples were completely melted by heating to 1473 K for 1 hr and allowed to cool slowly in the furnace by turning off the power supply. A second series was prepared in a similar way, but the molten material was solidified by quenching the reaction tubes into iced brine. Both these sets of samples had overall compositions ranging from 10 mole% PbS to 40 mole% PbS in 5 mole% steps and three other compositions containing 19, 21, and 22 mole% PbS.

A third series was prepared from mixtures of PbS and Sb_2S_3. These compounds were prepared by direct fusion of the elements in 20-g quantities, and checked by X-ray diffraction after reaction. Subsequently these materials were broken into granules, and mixed in the appropriate quantities to give samples of overall weight of 1 g. The mixtures were finely ground in an agate mortar, and pressed into pellets of 12 mm diameter and 2 mm thickness under a load of 108 kN for 60 sec. The pellets were sealed into evacuated silica tubes for subsequent reaction. Compositions ranging from 10 mole% PbS to 40 mole% PbS in 5 mole% steps and from 41 mole% PbS to 46 mole% PbS in 1 mole% steps were prepared. The samples were reacted at 748 K for 7 days.

In addition to these three series of samples, a few of the melt quenched preparations were annealed in evacuated silica tubes at 698 K for times varying between 1 hr and 7 days.

All samples were examined by powder X-ray diffraction using a Hägg–Guinier focusing camera and strictly monochromatic Cu$K\alpha_1$ radiation. The relative intensities of reflections were measured using a Joyce-Loebl double-beam recording microdensitometer. Lattice parameters were calculated and refined using the computer programs LAZY and PURUM written by Nord (*15*) and Werner (*16*).

Electron microscope samples were prepared by crushing representative pieces of each sample under *n*-butanol and allowing a drop of the resultant suspension to dry on a holey carbon film. Thin fragments whose edges projected over holes in the support

TABLE I

POWDER X-RAY DATA FOR ANNEALED SAMPLES OF Sb_2S_3

d_{obs} (nm)	Intensity[a]	*hkl*	d_{obs} (nm)	Intensity[a]	*hkl*
0.7940	10	101	0.2271	16	410
0.5640	30	200	0.2245	10	304
0.5597	13	002	0.2227	21	411
0.5035	47	201	0.2197	3	105
0.3973	27	202	0.2178	4	315
0.3622	31	011	0.2098	3	214
0.3565	60	301	0.2093	24	502
0.3543	73	103	0.2083	11	205
0.3448	33	111	0.1987	7	404
0.3168	13	210	0.1938	48	413
0.3122	25	302	0.1933	52	314
0.3102	29	203	0.1924	21	305
0.3044	100	112	0.1914	54	020
0.2757	85	212	0.1867	8	006
0.2717	4	104	0.1842	7	106
0.2673	58	013	0.1789	7	221
0.2600	28	113	0.1724	21	513
0.2523	35	402	0.1719	12	315
0.2509	17	204	0.1687	34	321
0.2420	18	312	0.1684	31	123

Note. Refined lattice parameters are $a = 1.1321$ nm, $b = 0.3846$ nm, $c = 1.1468$ nm (orthorhombic).

[a] Estimated from microdensitometer peak heights.

film were examined in a JEM 100B electron microscope fitted with a goniometer stage and operated at 100 kV.

Results

Characterization of Sb_2S_3

X-Ray diffraction. Three samples of stoichiometric Sb_2S_3 were examined, one was of fused material quenched from the melt, one from fused material slow cooled from the melt and one was of material annealed at 748 K for 7 days after fusion of the elements. All three samples gave X-ray powder patterns in good agreement with the data listed by the ASTM which was originally recorded by Swanson (*17*). However, our data contained more reflections than the ASTM data and some single reflections in this latter listing have been resolved into several lines in our study. Table I records the values found for the annealed samples. The unit cell parameters were refined on an orthorhombic cell with $a = 1.1321$ nm, $b = 0.3846$ nm, $c = 1.1468$ nm which compares well with the ASTM, viz. $a = 1.1229$ nm, $b = 1.1310$ nm, $c = 0.3839$ nm. The difference between the designations of the unit cell axes is because in this study we have followed the space group setting adopted by Bayliss and Nowacki (*5*).

It was noted that there were slight differences between the powder patterns of the three samples. The reflection indexed as {203} in the ASTM listing was found to have split into two or possibly three lines. Patterns from slow-cooled melt and quenched melt material showed two reflections which were indexed as {203} and {302} in this study. Powder patterns of the annealed material showed both these reflections to be diffuse with possibly a third reflection interposed with $d = 0.3110$ nm. In addition a new reflection with $d = 0.2178$ nm was only visible on powder patterns from annealed material and was indexed as {315}.

The powder pattern of material from a preparation with an overall reduced sulfur stoichiometry, $SbS_{1.4}$, showed no indication of disorder as the reflections were quite sharp. The powder pattern of this material was the same as that of annealed Sb_2S_3 with the same group of diffuse reflections described above present. Upon grinding, this sample revealed a single bead of free antimony of sufficient mass to account for the reduced stoichiometry, indicating that Sb_2S_3 has, at best, only a small composition range.

Electron microscopy. When projected down [010], Sb_2S_3 shows ribbons of the rocksalt structure related by glide reflection symmetry. Each ribbon is built up from half octahedra and four of these can be seen across the width of the ribbon. Because the electron scattering power of antimony is

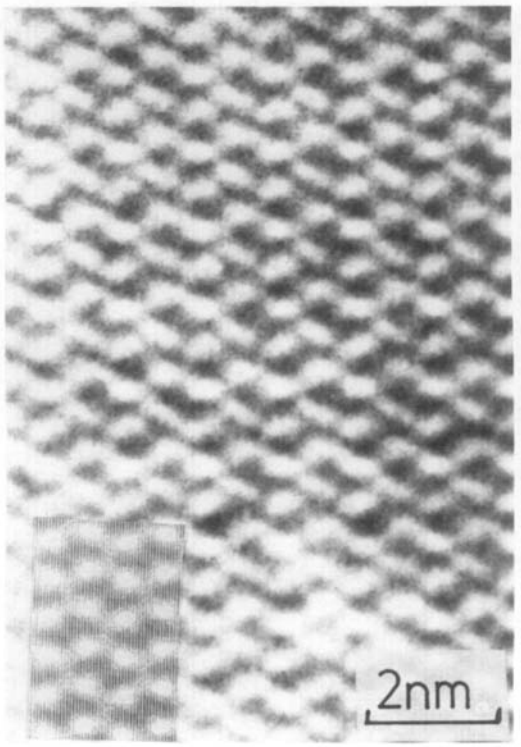

FIG. 2. Electron micrograph of Sb_2S_3 projected down the *b* axis. The ribbons of half octahedra are resolved as dark lozenge-shaped regions. The computed image of Sb_2S_3 is inset at bottom left.

much greater than that of the surrounding sulfur atoms, one can expect to see groups of darker intensity representing the four antimony atoms per ribbon unit. This was never achieved with the JEM 100B and the best image obtained of Sb_2S_3 from this instrument is shown in Fig. 2. The image clearly shows lozenge-shaped dense regions representing a cross section of each ribbon unit, but the antimony atoms are not resolved. Computer-simulated images for the ⟨010⟩ projection of Sb_2S_3 using experimental parameters relevant to the JEM 100B showed that the nearest match with the known arrangement of the antimony atoms occurred when the instrument was defocused in the region of −70 to −80 nm and this is shown inset in Fig. 2. Although it is clear that the metal atoms have not been resolved, it is possible to image the ribbon units and their arrangement.

Despite its inability to give atomic resolution, the JEM 100B was most useful for the purposes of phase analysis. In the context of undoped Sb_2S_3, this instrument was used to search for any planar defects intrinsic to this material. Despite a careful search, covering all three Sb_2S_3 samples prepared in this study, no faults were found. This search was extended to material originating from a sample with reduced sulfur stoichiometry, $SbS_{1.4}$, with identical results.

Phase Analysis of Sb_2S_3 Reacted with PbS: Material Prepared by Sintering Sb_2S_3 and PbS

X-Ray diffraction. Examination of the powder patterns showed that a two-phase equilibrium existed between Sb_2S_3 and Sb_2S_3 doped with approximately 45 mole% PbS. Powder patterns of material containing 43–45 mole% PbS revealed a pure phase. This was identified as the synthetic counterpart to the mineral zinckenite, $PbSb_2S_4$, by reference to the ASTM index (*18*) which is in reasonable agreement with the powder pattern obtained in this study. At PbS concentrations in excess of 45 mole%, a new set of reflections was observed together with those of zinckenite. No lattice parameter shifts or stoichiometry ranges were observed in the powder patterns of Sb_2S_3 from these preparations. The phase analysis is summarized in Table II.

Electron microscopy. A number of samples containing up to 50 mole% PbS were selected for examination by electron microscopy. This confirmed that a two-phase series existed up to approximately 43 mole% PbS. The electron diffraction patterns showed that only Sb_2S_3 and zinckenite occurred across this range of PbS concentration. Many crystals were examined at a relatively low magnification in order to seek for defects such as planar faults. Despite an

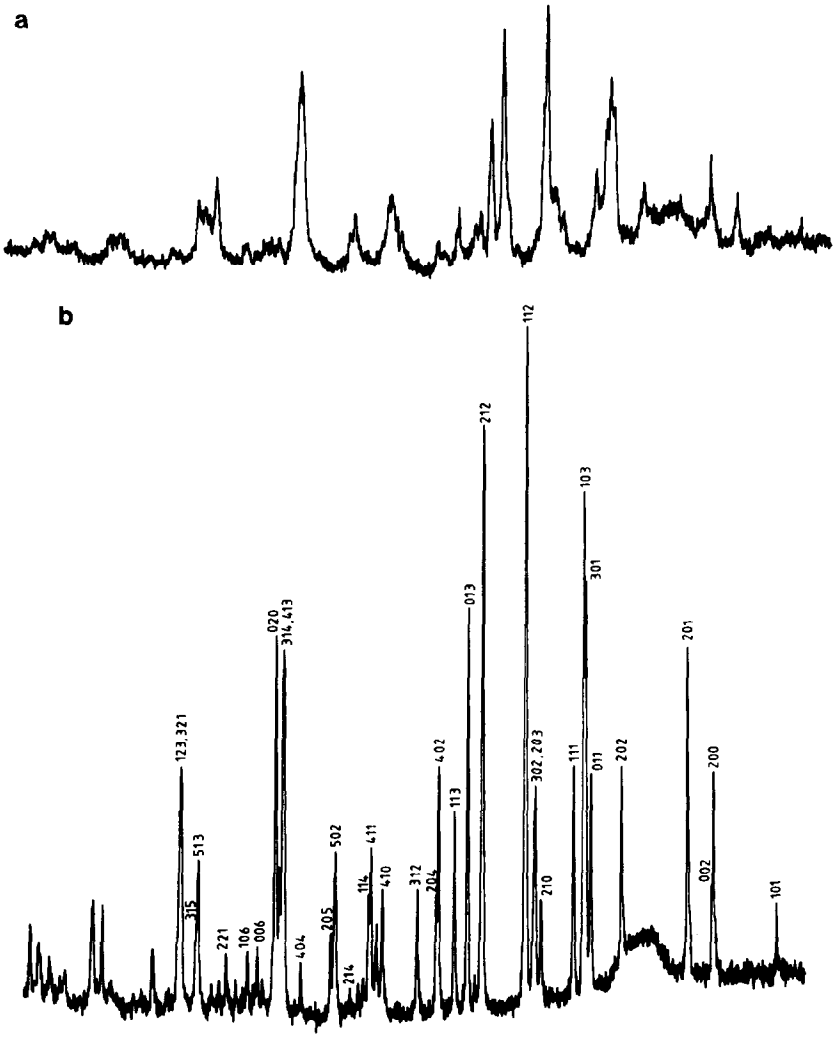

FIG. 3. (a) Diffractometer trace of the X-ray powder pattern of Sb_2S_3 reacted with 20 mole% PbS cooled slowly from the melt, compared to that of pure Sb_2S_3 shown in (b).

extensive search, no crystals were found to contain faults or intergrowths between Sb_2S_3 and zinckenite. However, the diffraction patterns of crystals of zinckenite projected down ⟨001⟩ revealed the presence of a weak superlattice which is reported in more detail in a separate publication (*19*).

Material Prepared by Slow Cooling from the Melt

X-Ray diffraction. Compared to material which had been prepared by the solid-state reaction of Sb_2S_3 with PbS, this series of samples showed marked differences in their powder patterns. At low (approximately 10 mole% PbS) doping levels new reflections were observed but these could not be ascribed to the phase zinckenite or any other previously reported phase in the system. Although no overall lattice parameter shift could be observed, some slight relative shifts between reflections could be detected in the Sb_2S_3 powder pattern.

At approximately 20 mole% PbS concen-

TABLE II

X-RAY PHASE ANALYSIS OF SINTERED Sb_2S_3–PbS MATERIALS

mole% PbS	Phases present	Comments
10	Sb_2S_3 + zinckenite	
15	Sb_2S_3 + zinckenite	
20	Sb_2S_3 + zinckenite	
25	Zinckenite + Sb_2S_3	Zinckenite now the major phase present
30	Zinckenite + Sb_2S_3	The zinckenite reflections now appear to be slightly more diffuse than in previous sample
35	Zinckenite + Sb_2S_3	The zinckenite reflections are not quite so diffuse as in the 30 mole% sample
40	Zinckenite + trace Sb_2S_3	All zinckenite reflections are now sharp
42	Zinckenite	No observable Sb_2S_3
43	Zinckenite	No observable Sb_2S_3
44	Zinckenite	No observable Sb_2S_3
45	Zinckenite	No observable Sb_2S_3
46	Zinckenite	No observable Sb_2S_3, but reflections from another unidentified phase observed

tration, the powder pattern revealed a very disordered material. Although the overall appearance of the pattern was similar to the pattern of pure Sb_2S_3, the reflections were very broad and diffuse. A densitometer trace of the powder pattern of this material is shown in Fig. 3a together with a trace of pure Sb_2S_3 in Fig. 3b.

When the doping level was increased to 30 mole% PbS, the powder pattern revealed a mixture of zinckenite and Sb_2S_3 with the former as the major phase. In these materials, however, no trace of disorder could be detected and all reflections appeared quite sharp.

When the amount of PbS reached greater doping levels, 40 mole% and beyond, neither zinckenite nor Sb_2S_3 could be detected. The powder patterns appeared multiphase with sharp reflections which were not identified. The phase analysis of this series of samples is summarized in Table III.

Electron microscopy. At low PbS concentrations of approximately 10 mole%, all crystals gave diffraction patterns corresponding to Sb_2S_3. No crystals of the phase zinckenite were found. Some local disorder was found in the crystals of Sb_2S_3 in the form of small, roughly spherical regions of darker contrast when projected down the *b* axis. These faults or "cluster" defects were approximately 1.5 nm across and were relatively sparsely distributed. Figure 4 shows such a cluster isolated within a crystal of Sb_2S_3. Fragments of Sb_2S_3 projected down [001] appear to show these clusters in elevation and measurements reveal that they are some 10–12 nm long. When the PbS concentration was raised to 20 mole%, many highly disordered crystals were found. Certain clues as to the nature of the disorder were given in crystals projected such that their diffraction patterns were of the systematic type. The medium resolution images then showed heavy planar faulting with some partial ordering as shown in Fig. 5. The corresponding diffraction patterns were heavily streaked.

Comparison of such diffraction patterns with similar patterns from undoped Sb_2S_3 showed that it was still possible to recognize the basic Sb_2S_3 pattern even in the most disordered cases, as seen in Figs. 6a and b. Examination of these two diffraction patterns showed that the disorder appears to have concentrated intensity into the same positions as the subcell modulations seen in the pattern from undoped Sb_2S_3, suggesting that the nature of the disorder is

TABLE III

X-RAY PHASE ANALYSIS OF SLOW-COOLED MATERIAL

mole% PbS	Phases present	Comments
10	Sb_2S_3 + unknown	Several very faint and diffuse reflections appearing at low angles
20	Sb_2S_3?	Very diffuse, some resemblance to the pure Sb_2S_3 pattern
30	Zinckenite + Sb_2S_3	No evidence of disorder—sharp reflections
40	Complex, multiphase	Phases not identified. No zinckenite or Sb_2S_3
50	Complex, multiphase	As 40 mole% sample

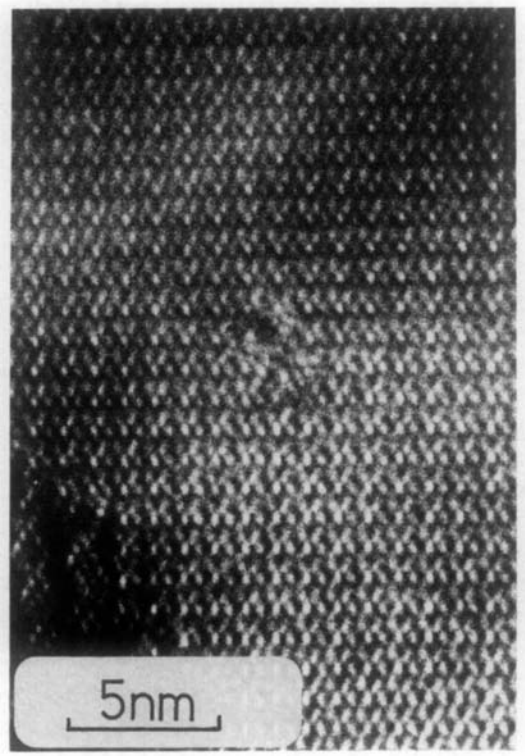

FIG. 4. Electron micrograph, viewed parallel to (010) of a crystal fragment from a sample of overall composition 90 mole% Sb_2S_3 : 10 mole% PbS slow cooled from the melt, showing a cluster defect centrally.

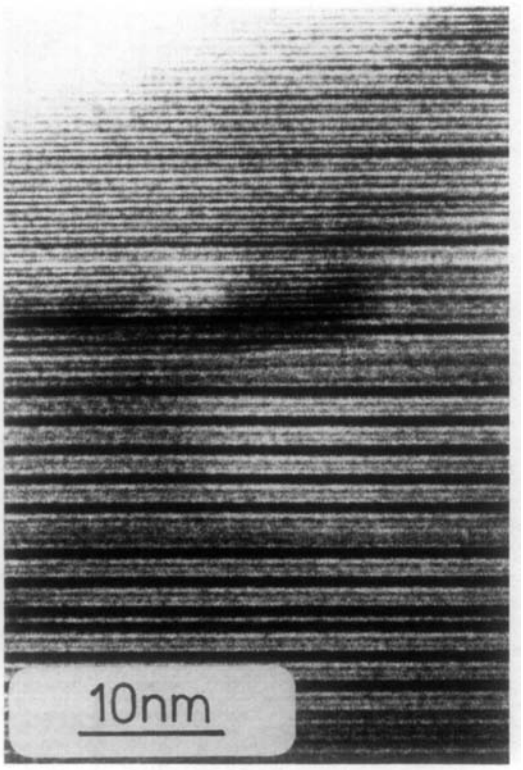

FIG. 5. Electron micrograph of a heavily faulted crystal from a sample of overall composition 30 mole% Sb_2S_3 : 20 mole% PbS slow cooled from the melt. Partial ordering of the faulting is apparent.

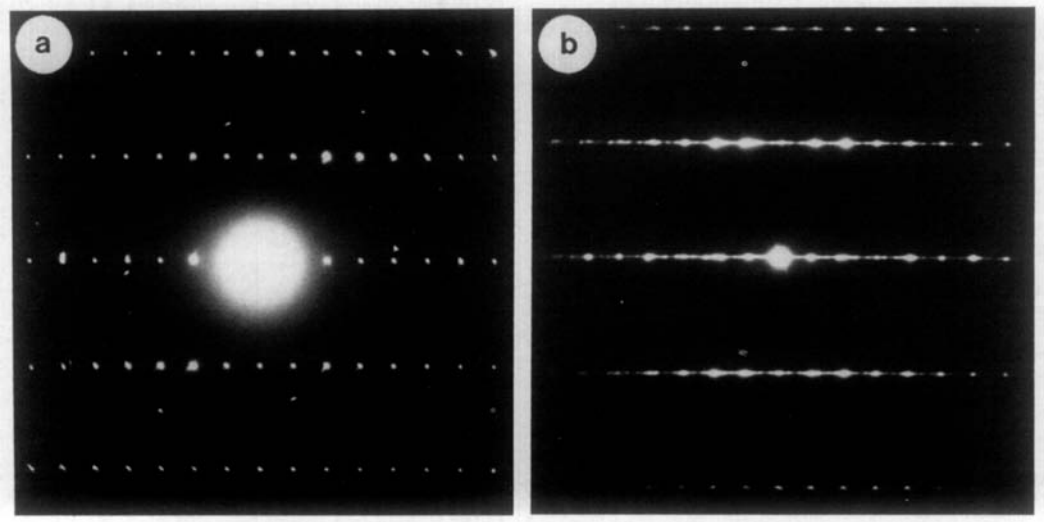

FIG. 6. (a) Electron diffraction pattern of Sb_2S_3 projected down (001) compared to (b) the electron diffraction pattern from the crystal shown in Fig. 5. The similarity between the patterns is striking.

closely related to the structure of Sb_2S_3 itself. The direction of the streaking occurred along ⟨100⟩* indicating that faulting lay on {100} planes. Comparison of medium-resolution images for both Sb_2S_3 and disordered crystals taken with the same type of orientation appear to show an intergrowth of Sb_2S_3 with unknown material as shown in Figs. 7a and b, respectively. At this stage it was impossible to say whether this represents a genuinely new structure or merely a quasiordered intergrowth of Sb_2S_3 with the phase zinckenite.

The maximum level of PbS concentration studied by electron microscopy for this series of preparations was 30 mole% and in these only Sb_2S_3 and zinckenite crystals were found with no evidence of disorder. Crystals of zinckenite projected down ⟨001⟩ did not show diffraction patterns having the weak superlattices as found in the sintered preparations.

Material Prepared by Fast Quenching from the Melt

X-Ray diffraction. The X-ray powder patterns of melt quenched material differed from the patterns obtained for material of similar compositions prepared by sintering. No trace of the phase zinckenite was detected over the range of PbS concentration, which was from 0 to 40 mole%.

For material containing 10 mole% PbS, a definite and uniform lattice parameter shift was observed in the pattern of the Sb_2S_3 reflections. This indicated a clear increase in all three cell parameters. All of the reflections observed in the pattern of undoped Sb_2S_3 were present in the pattern of the doped material. There was no evidence for any disordering of the Sb_2S_3 structure, although the {101} reflection was now weaker. In contrast to slow-cooled material of similar composition, no new reflections were observed.

At the slightly higher concentration of 15 mole% PbS the comparison between quenched alloy and Sb_2S_3 powder patterns was more complex. Although the overall appearance of the powder pattern from doped material appeared very similar to that of the pattern of undoped Sb_2S_3, the reflections were now weaker and more diffuse in character. It was also noticed that for $d < 0.25$ nm the quenched alloy pattern differed from the undoped Sb_2S_3 pattern.

Although many high angle reflections were either absent or too diffuse to measure accurately, enough low angle reflections were indexed to refine the unit cell parameters. This is presented in Table IV showing d values for the doped (15 mole% PbS) and undoped materials. It is clear that the unit cell has contracted along the a and c directions by 0.34 and 1.88%, respectively, while the b parameter has remained relatively unchanged (−0.03%). However, more data will be required to establish

TABLE IV

X-RAY POWDER DATA AND REFINED CELL PARAMETERS OF THE Sb_2S_3 REFLECTIONS IN THE SAMPLE 85 mole% Sb_2S_3: 15 mole% PbS MELT QUENCHED, COMPARED WITH THOSE IN PURE Sb_2S_3

hkl	Pure Sb_2S_3, d_{obs} (nm)	85 mole% Sb_2S_3 : 15 mole% PbS
101	0.7940	0.7906
200	0.5640	0.5642
002	0.5597	0.5583
201	0.5035	0.5028
202	0.3973	0.3967
011	0.3622	0.3637
301	0.3565	0.3563
103	0.3542	0.3545
111	0.3448	0.3460
112	0.3044	0.3050
212	0.2757	0.2763
013	0.2673	0.2678
402	0.2523	0.2518

Note. Refinement of the orthorhombic unit cell gave: (a) for pure Sb_2S_3; $a = 1.1321$ nm, $b = 0.3846$ nm, $c = 1.1408$ nm; (b) for 85 mole% Sb_2S_3 : 15 mole% PbS; $a = 1.1276$ nm, $b = 0.3845$ nm, $c = 1.1194$ nm.

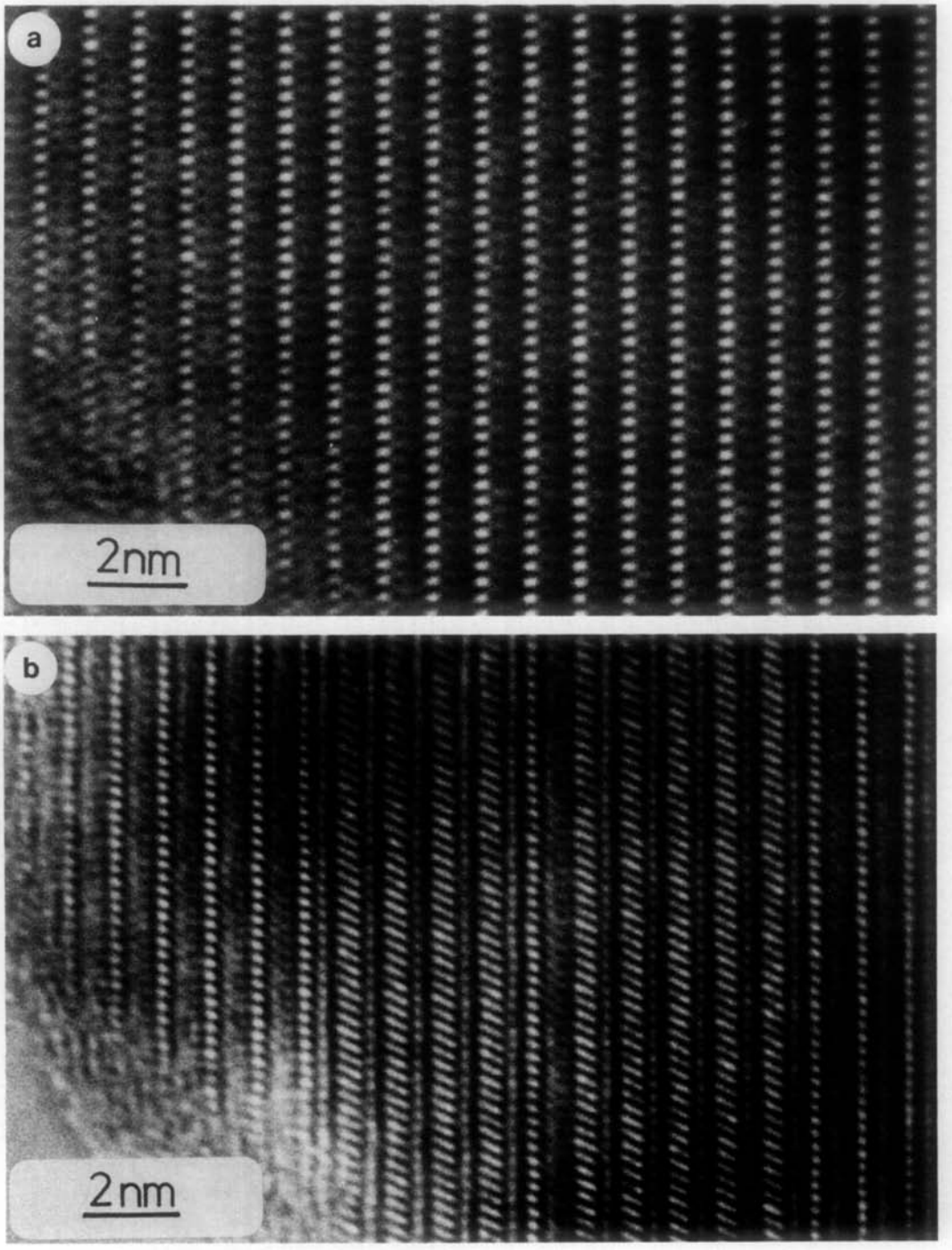

FIG. 7. (a) Electron micrograph of crystal of Sb_2S_3 projected down [001]. (b) Similar projection of a crystal from a sample of overall composition 80 mole% Sb_2S_3 : 20 mole% PbS, showing intergrowth of Sb_2S_3-like regions with new material.

TABLE V

X-RAY ANALYSIS OF QUENCHED Sb_2S_3–PbS

mole% PbS	Remarks
10	Appears to be pure Sb_2S_3 but with a small positive lattice parameter shift. All reflections appear sharp
15	Pattern of Sb_2S_3 is still visible but all reflections are diffuse
19	Similar to the Sb_2S_3 pattern in intensity and position but reflections are very diffuse
20	Similar to 19 mole% sample
21	Similar to the 19, 20, and 21 mole% samples
25	Still a very diffuse and weak pattern but looks less like Sb_2S_3 than the powder patterns from material of lower PbS concentration
30	Quite different to the powder patterns described above. Some diffuse intensity remains but most reflections are sharp. There appears to be more than one ordered phase present. These were not identified
35	Very similar to the 30 mole% sample
40	Powder pattern shows unidentified ordered phases unlike those observed in the 30 and 35 mole% samples

whether this varied systematically with nominal dopant concentration.

Although the overall pattern of intensities was still similar to that of undoped Sb_2S_3 for PbS concentrations of between 19 and 25 mole%, the powder patterns showed very diffuse reflections. Some reflections, notably {020}, appeared to remain relatively sharp and intense across this range of doping while others such as {101} had virtually vanished.

The powder patterns of Sb_2S_3 reacted with 30, 35, and 40 mole% PbS showed little similarity to those patterns obtained from material having lower PbS concentrations. The reflections were once again seen to be sharp with little sign of diffuse intensity. The complexity of the patterns suggested that more than one phase was present but these phases could not be characterized.

The X-ray phase analysis is summarized in Table V. Because no ordered discrete phases were identified, only general remarks are given.

Electron microscopy. This material contained the greatest variety of defect structures encountered in the study. When Sb_2S_3 was reacted with 10 mole% PbS, the crystals appeared to show a relatively high density of the cluster type of defect as observed to occur in slowly cooled material of similar composition. The clusters appear to be of similar shape and size as those reported for the slow-cooled sample. The average cluster spacing is of the order of 8 nm and appears to be randomly distributed. The clusters appear somewhat variable in contrast, which may reflect some variability in their internal structure. It can also be noted that, in some crystal fragments, short lengths of planar faults have formed on {100} planes of Sb_2S_3. No crystals of the phase zinckenite were found in this sample.

Increasing the PbS concentration to 15 mole% resulted in a sample containing a variety of different defect structures. Some crystals showed only the cluster type of defect as represented earlier. The average diameter of the clusters was gauged to be approximately 1.5 nm, much the same as those observed in samples of lower PbS concentration. However, the spacing of these clusters is now reduced to the order of 5 nm. Such a crystal is shown in Fig. 8. The contrast of these clusters can be seen to change from light to dark between the thinner and thicker parts of the crystal. Although the lattice image does not show direct atomic resolution of the metal positions, the ribbon type structural units of Sb_2S_3 can be discerned where the crystal is thinner at the edge. The appearance of the defective areas gives rise to the suggestion that certain ribbon units have become extended in width for a limited region of crys-

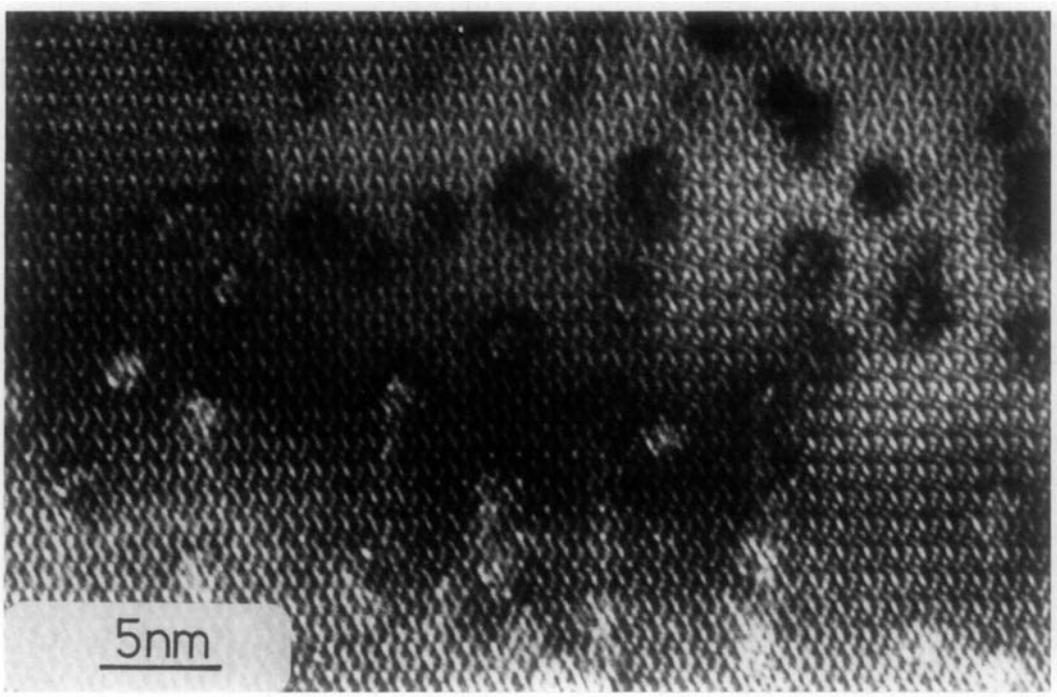

FIG. 8. Cluster defects in a crystal fragment from a sample of overall composition 85 mole% Sb_2S_3 : 15 mole% PbS, rapidly quenched from the melt, projected down [001]. The contrast of the clusters is seen to change from light, near the crystal edge at the bottom of the micrograph, to dark in the thicker regions near the top.

tal. These observations would appear to show that it would be unreasonable to interpret such entities as mere holes in the Sb_2S_3 matrix.

The most common faults found in crystals from material containing 15 mole% PbS were observed on {101} planes of the Sb_2S_3 matrix. A good example of this kind of faulting is shown in Fig. 9a. The accompanying diffraction pattern shown in Fig. 9b reveals a well-defined superlattice. A few cluster defects can be seen in the image but the main feature is the rather broad bands of different contrast alternating with layers of Sb_2S_3. Because of this appearance, such faults would be better regarded as intergrowths as they seem to constitute slabs of new material intergrown between layers of Sb_2S_3. Measurements of many individual intergrowths show that they always have the same width but that their spacing varies from a minimum of about 2 nm up to approximately 9 nm.

Many of the crystals found in material containing 15 mole% PbS appeared to be Sb_2S_3, but heavily faulted on {100} planes as shown in Fig. 10. The diffraction patterns obtained from such crystal fragments showed a marked resemblance to that of the ⟨010⟩ projection of perfect Sb_2S_3. Although the subcell reflections of Sb_2S_3 could be recognized, the finer details of the pattern varied from streaking to superlattice spotting, always along [100]* as seen in

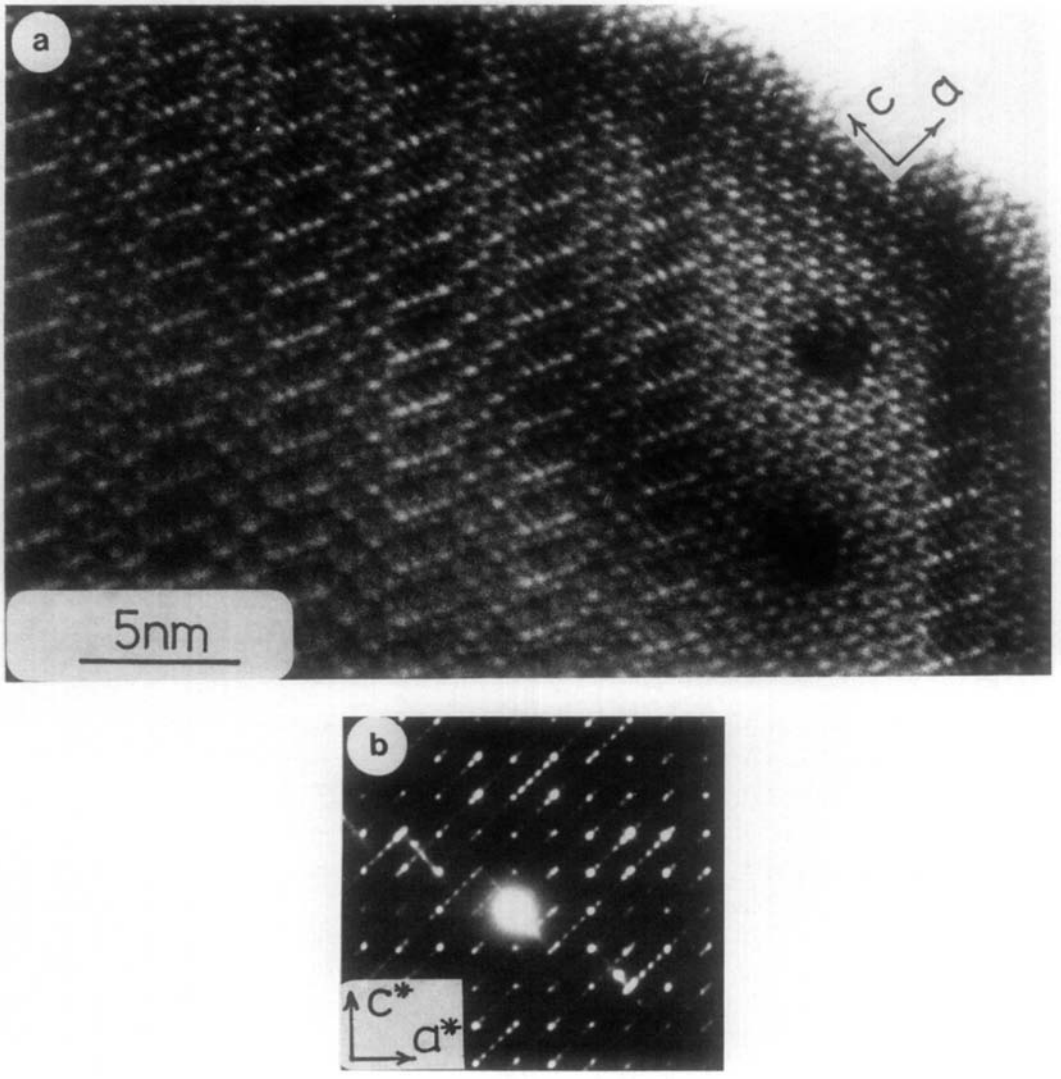

FIG. 9. (a) Electron micrograph of a crystal fragment from a sample of overall composition 85 mole% Sb_2S_3 : 15 mole% PbS showing Sb_2S_3 intergrown with a new structure along (101). The intergrowths are partly ordered. Two cluster defects show as dark patches within the SbS_3 matrix. The axes marked refer to this part of the crystal. (b) Electron diffraction pattern of the crystal in (a). The axes marked refer to the Sb_2S_3 cell. The superlattice reflections along (101) reveal the intergrowths to be well ordered over much of the crystal.

Figs. 11a, b, and c. Such variability may be explained as an array of closely spaced faults or intergrowths, sometimes ordered, on {100} planes in an Sb_2S_3 matrix. The fact that the Sb_2S_3 subcell modulations are always easily visible suggests that such faulting takes the form of intergrowths of new material closely related in structure to that of Sb_2S_3 and is in keeping with earlier observations.

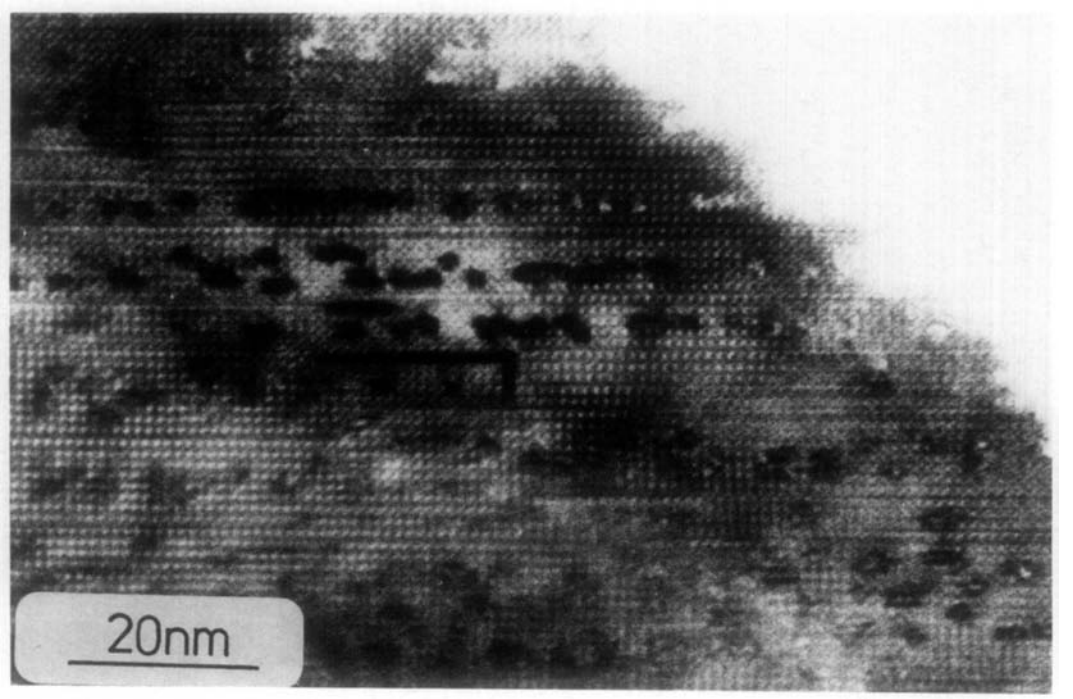

FIG. 10. Electron micrograph of a crystal fragment from a sample of overall composition 85 mole% Sb_2S_3 : 15 mole% PbS, heavily faulted on (100) and containing many cluster defects. The crystal is projected down the b^* axis.

A few crystals found in the 15 mole% PbS sample appeared to show considerable disorder as shown in Fig. 12. Ordered regions of Sb_2S_3 can be seen away from the fragment edge but complex disordering of the Sb_2S_3 ribbon units appears to have taken place over part of the crystal. It would be reasonable to suggest that ordering in the direction of crystal projection, i.e., along ⟨010⟩ Sb_2S_3, still existed.

When the PbS concentration was raised to 20 mole% most crystals found were Sb_2S_3 heavily faulted on {100} planes although a few fragments of Sb_2S_3 containing quasiordered intergrowths on {101} were recorded. Some crystals contained alternate bands of {101} intergrowths and cluster defects in an Sb_2S_3 matrix. All three types of defect can be seen in Fig. 13. A number of clusters have joined along ⟨001⟩ to form a pseudoplanar fault, as seen in this photograph.

At the 25 mole% PbS concentration the only crystals found were those heavily faulted on {100} planes of Sb_2S_3. A typical fragment of this material is shown in Fig. 14. Although the image does not permit direct interpretation of the structure, the position of the faults appears to be delineated by the darker wavy fringes. The diffraction patterns of these crystals, although heavily streaked, still show a strong resemblance to the pattern of Sb_2S_3 when projected down ⟨010⟩.

The most heavily doped sample of Sb_2S_3 examined by electron microscopy, 30 mole% PbS, showed that about half the crystals found were of the disordered Sb_2S_3 variety, mostly with faulting on {100} planes as shown in Fig. 15. Limited ordering of the

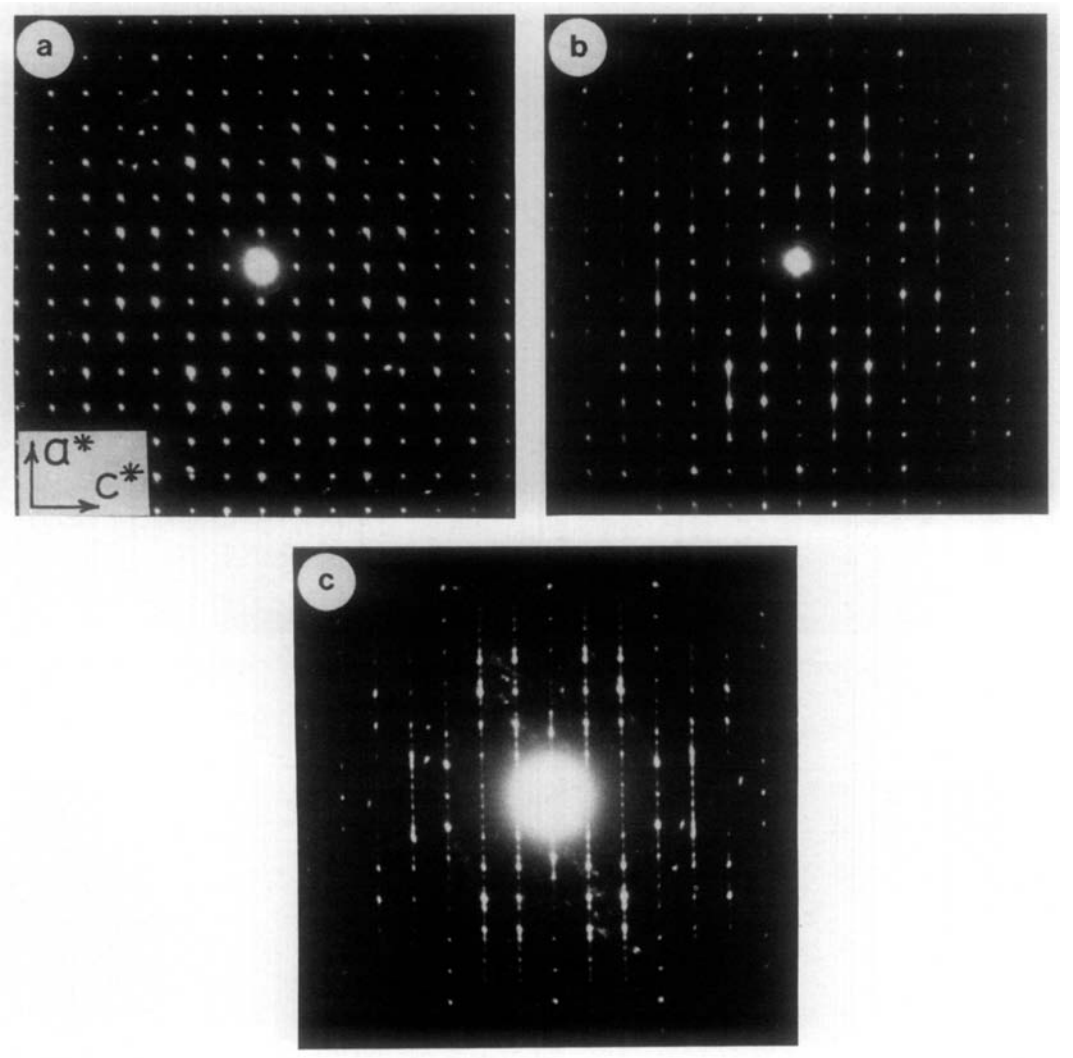

FIG. 11. Electron diffraction pattern from (a) Sb_2S_3 compared to diffraction patterns from crystals of the type shown in Fig. 10, with smaller, (b), or greater, (c), degrees of faulting on {100}. In (c) quite well formed superlattice spots are to be seen, indicating that the faults are reasonably well ordered.

faults occasionally occurred. The other material in this sample was found to be a previously unreported phase, free of defects. The structure of this compound will be reported elsewhere.

Finally we record that in these rapidly cooled materials, a glass sometimes formed in samples of composition 20 mole% PbS, which is close to the eutectic (*3*).

Discussion

X-Ray Diffraction

The X-ray powder diffraction results are complex, and although the X-ray camera used was a high-resolution instrument, it was impossible to interpret the data in terms of real structures. However, a great deal of information at an intermediate level

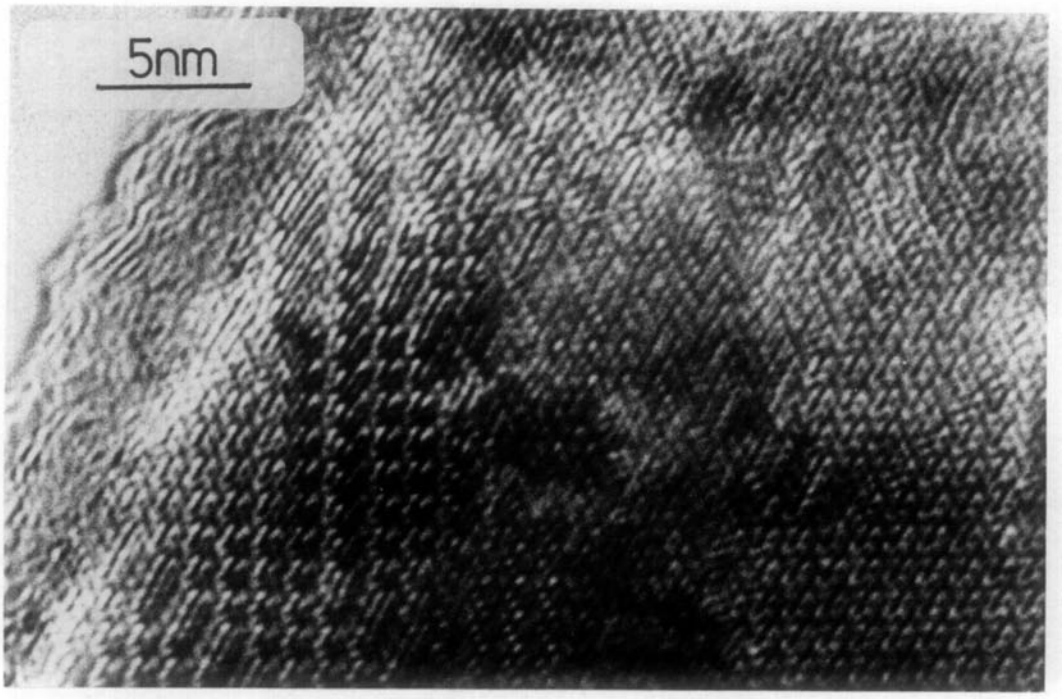

FIG. 12. Micrograph showing a very disordered crystal from a sample of overall composition 85 mole% Sb_2S_3 : 15 mole% PbS quenched from the melt. Well-ordered Sb_2S_3, projected down the *b* axis, is seen in the lower right. Disordered intergrowths on {101} can be found in other parts of the micrographs.

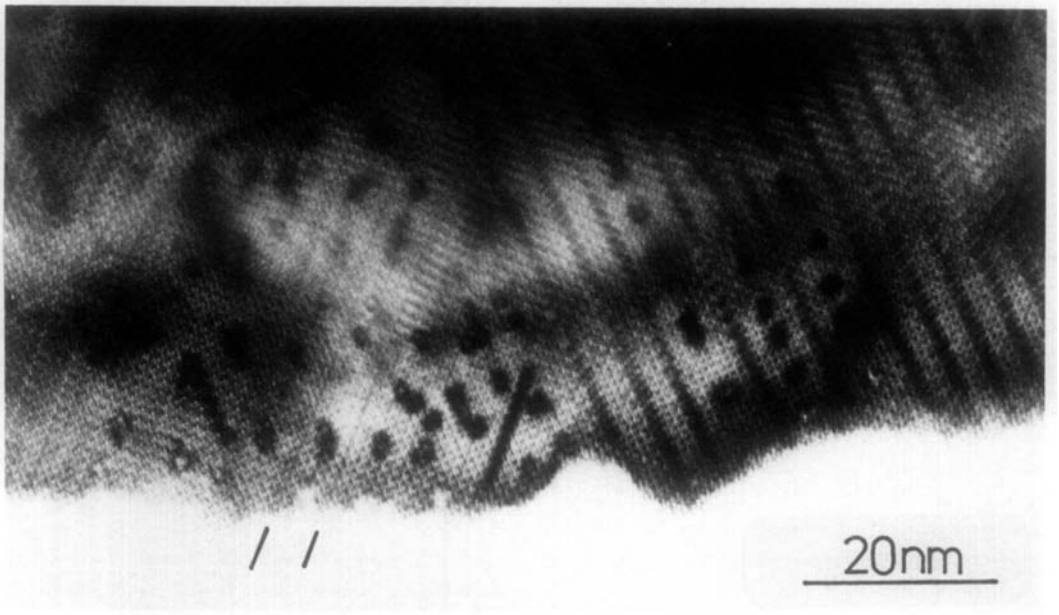

FIG. 13. Micrograph of a disordered crystal from a sample of overall composition 80 mole% Sb_2S_3 : 20 mole% PbS, projected down *b*. Partly ordered defects on {101} can be seen on the right, and {100} faults, two of which are marked, on the left. Cluster defects, (dark patches) occur in the Sb_2S_3 matrix.

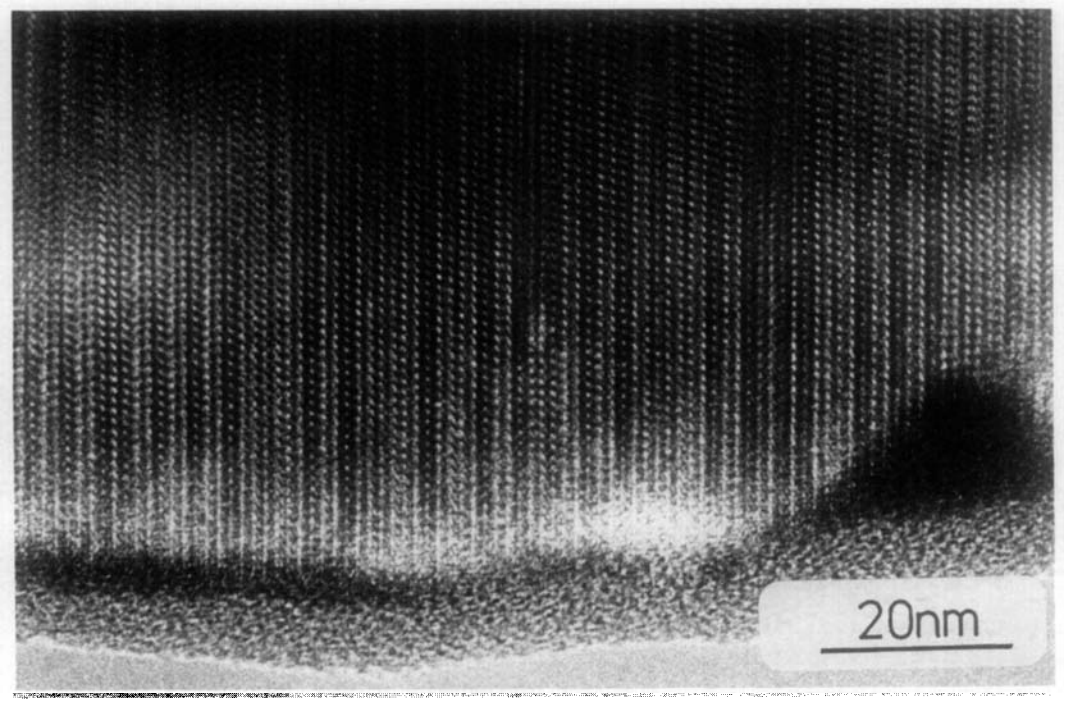

FIG. 14. Micrograph of a crystal from a sample of overall composition 75 mole% Sb_2S_3 : 25 mole% PbS containing a large concentration of {100} faults.

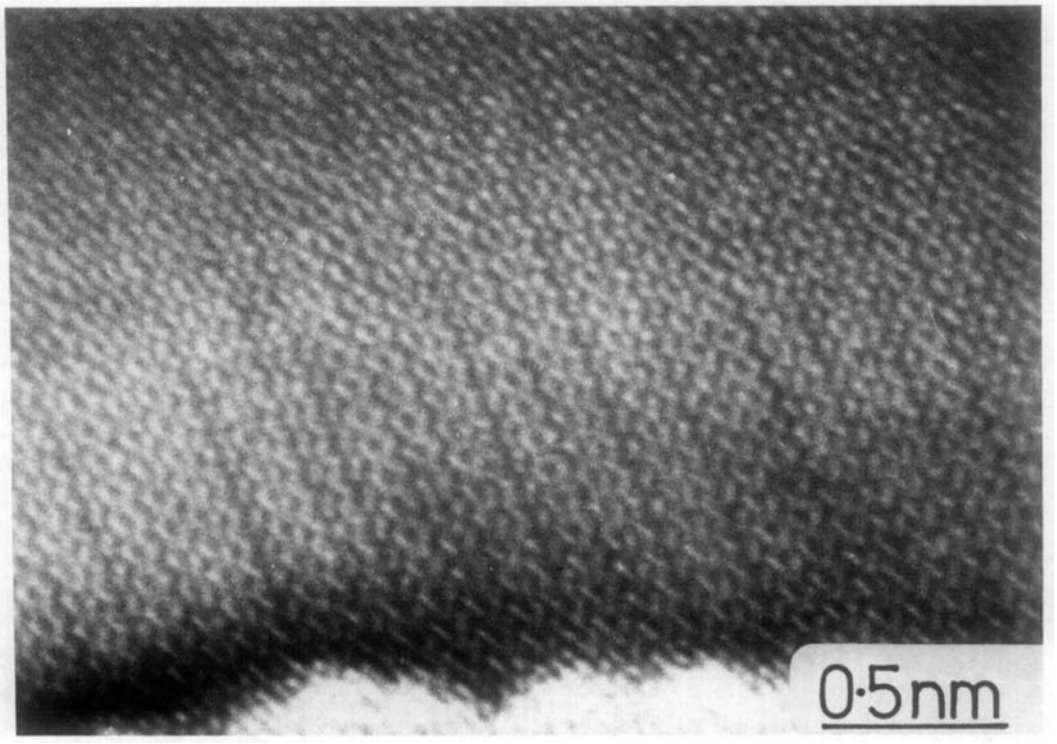

FIG. 15. Micrograph of a crystal from a sample of overall composition 70 mole% Sb_2S_3 : 30 mole% PbS containing a large concentration of {100} faults, projected down the *b* axis.

of discrimination, somewhere between optical microscopy and electron microscopy, was amassed. This is worthy of consideration in this section, not only for the information which can be obtained from the X-ray films, but also in conjunction with the electron microscope results which are considered below.

Careful comparison of X-ray films from stoichiometric Sb_2S_3 show slight differences, depending upon the heat treatment accorded to the samples. These differences are small and no obvious structural reasons for such changes could be found during electron microscope examination. We will not consider these small differences in this paper, but suggest that the X-ray data from the annealed material, presented in Table I, is probably the most reliable that we have obtained.

The X-ray powder analysis of sintered samples reveals a classical two-phase region. One phase was Sb_2S_3, with no apparent stoichiometry range, whereas the other was found to be zinckenite. This latter material appears to have a small stoichiometry range based upon both lattice parameter shifts and the appearance of only zinckenite reflections on a few films from samples of varying composition. The problem of the stoichiometry range of zinckenite is not central to the subject matter of this paper and will be discussed in another publication (*19*).

The X-ray results so far summarized show that Sb_2S_3, prepared under the conditions described here, is a stoichometric compound with little ability to incorporate PbS into its structure. However, the results obtained from quenched or slowly cooled melts show a quite different behavior. Although we do not know the structure of the melt, we can see that the rate of cooling has a great influence on the way that this structure is transformed into solid phases. Consider the slowly cooled material first. A clear distinction occurs at the eutectic point. In samples between Sb_2S_3 and the eutectic, a product forms which we can loosely describe as Sb_2S_3. To be sure, the X-ray results show that the material is very disordered. Nevertheless, the powder patterns bear an overall resemblance to that of pure Sb_2S_3, and no other phases are present. This suggests that the melt is fairly homogeneous, and that on cooling, it crystallizes homogeneously.

The PbS component is taken into the Sb_2S_3 structure, which is, as a consequence, severely disrupted. This does not agree with the classical liquidus and solidus form of the phase diagram shown by Salanci (*14*), but such phase diagrams refer to equilibrium situations, and we are unlikely to be close to equilibrium in this situation.

On the zinckenite side of the eutectic the reverse is true. The X-ray diagrams are sharp and show only zinckenite and Sb_2S_3. This suggests that zinckenite nucleates and as the melt solidifies, the composition of the liquid moves toward the eutectic in a classical fashion. At the eutectic, both zinckenite and pure Sb_2S_3 are then precipitated.

In the rapidly quenched material a similar pattern of behavior was found on the basis of X-ray data. At compositions on the Sb_2S_3 side of the eutectic, the powder patterns resembled Sb_2S_3, but with diffuseness of reflections and apparent lattice parameter shifts. On the zinckenite side of the eutectic the reflections are sharp. No zinckenite was present, even in samples containing 40 mole% PbS. The phase or phases that were present could not be determined from the X-ray powder data. Classical methods of incremental variation of the composition coupled with a careful examination of intensities of the X-ray lines was unsatisfactory in these nonequilibrium samples.

The difference in behavior on either side of the eutectic is marked, and reveals that nucleation of zinckenite or of other ordered phases is a precise reaction, requiring the correct ratio of Pb, Sb, and S for success.

On the Sb_2S_3 side of the eutectic, however, pure Sb_2S_3 does not appear to nucleate at all, as no sharp reflections from Sb_2S_3 were found in this region. Clearly X-ray analysis suggests that the Sb_2S_3 structure is flexible enough to incorporate quite massive amounts of PbS and that structural or free energy changes on crystallization are not great enough to produce phase separation into Sb_2S_3 and a liquid richer in PbS. The structural reason for this may lie in the fact that the Sb_2S_3 structure is composed of square pyramids of five S atoms surrounding an Sb atom, with the lone-pair electrons of the Sb forming a sixth apex to the pyramid, converting it into a distorted octahedron. The Pb atoms naturally adopt an octahedral configuration, and can fit into such a structural scheme. Moreover, if we assign a valence of 2 to Pb, the Pb^{2+} ions would also possess a lone pair of electrons, completing the Sb_2S_3 framework. Such a partial replacement or substitution of Sb by Pb would certainly result in lattice parameter changes, and a change in the sharpness and intensity of the reflections in powder X-ray diffraction patterns. This analogy cannot be taken far at this stage, but it is presented to show that a model which is in accord with X-ray observations can be evolved for the structure of the material which is in accord with X-ray observations.

Electron Microscopy

The electron microscope results complement the X-ray data in that they provide direct information on the defect structure of crystallites without giving an overall picture of the order or disorder present in the base structure of the sample. Thus, in the samples prepared by sintering PbS with Sb_2S_3, no disorder was found in either the Sb_2S_3 or zinckenite present.

An examination of slow-cooled materials reveals the nature of the disorder which caused the degradation in quality of the X-ray powder photographs in the Sb_2S_3 part of the phase region. The material is clearly Sb_2S_3, according to electron diffraction data, but the structure is severely broken up by two sorts of defects. In samples containing low concentrations of PbS, up to 10 mole%, the defects consist solely of small clusters of disordered material, approximately spherical in shape, and of diameters of about 1.5 nm. At higher concentrations of PbS, faulting occurs on (100) planes. It would appear that these faults are often partially ordered, so that we have what would appear to be a new structure intergrown with the Sb_2S_3 structure. The coherent plane between the two structures is (100). Beyond the eutectic, electron microscopy showed only well-ordered Sb_2S_3 and zinckenite, in accord with the X-ray data.

The fast-cooled material showed greatest disorder in the Sb_2S_3 crystals, but a pattern of behavior similar to that in the slow-cooled material was observed. At low overall concentrations of PbS, the cluster defects were found. The size of these defects was, as found in the samples which were slow cooled, about 1.5 nm. The spacing of the defects varied with overall PbS concentration, as one would expect, with higher PbS concentrations producing greater concentrations of defects. At PbS concentrations of 20 and 25 mole% the defects found were {100} faults, as recorded in the slow-cooled material. These faults were never well ordered, although vestiges of ordering were sometimes detectable.

In contrast to the slow-cooled material, a new defect type was found in the quench cooled samples. It lies in the composition region between that where the cluster defects form and that where the {100} faults predominate. These new defects were lamellae of a new structure, coherently intergrown with the Sb_2S_3 matrix along {101} planes. There was quite a lot of evidence for the ordering of these lamellae, and

sometimes a distinct superlattice was observed on the electron diffraction patterns of faulted crystals. In such cases, the spacing of the lamellae was regular within the Sb_2S_3 structure. However, the nonequilibrium nature of these samples means that no hard and fast boundaries occur between the different regions.

General Conclusions

Material prepared in this study under conditions close to equilibrium, i.e., by sintering PbS and Sb_2S_3 mixtures, compared well with the findings of Craig *et al.* (*11*) and Salanci (*14*) in that only two phases, zinckenite and Sb_2S_3, were found to exist over the greater part of the PbS concentrations investigated. However, the results gained in the present investigation show that despite the simple appearance of the published equilibrium phase diagram, Sb_2S_3 can accommodate considerable amounts of PbS into its structure under nonequilibrium conditions. This is able to take place up to the eutectic composition of about 23 mole% PbS. The PbS is incorporated into the Sb_2S_3 structure in three ways. At lower amounts of PbS, clusters of new structure form, coherently intergrown in the Sb_2S_3 matrix. At somewhat larger concentrations and higher temperatures, lamellae of a new structure grow coherently into the Sb_2S_3 structure. The coherence is along {101} planes, and partial ordering of these lamellae is not uncommon, even in such rapidly formed materials. At greater PbS concentrations, faulting along {100} planes is found. These planar faults are not found to order readily. X-Ray diffraction reveals that the lattice parameters of the disordered Sb_2S_3 phase do increase, but these changes are difficult to quantify in the disordered samples examined in this study, and impossible to relate directly to the microstructures of the crystals. An interpretation of such changes in terms of point defects is not justified.

Such faulting was not detected in the studies of either Craig *et al.* (*11*) or Salanci (*14*). This does not necessarily mean that their samples did not contain defects but probably reflects the lower resolution obtained using X-ray methods instead of electron microscopy. Because faulted material was only observed in this study in samples prepared under nonequilibrium conditions such as quenching from the melt, there is the possibility that such structures may exist in ordered forms at temperatures close to the solidus analogous to the so-called V-phases (*20*) found to occur in the PbS–Bi_2S_3 system close to Bi_2S_3.

The structure of these defects is of considerable interest. The resolution of the electron microscope used did not allow us to obtain unequivocal data on this point, but suggested that the defects could well consist of chains of (Sb, Pb)S_5 square pyramids that were of different dimensions to those found in Sb_2S_3. A high-resolution electron microscope study to further clarify this suggestion will form the basis of a future publication (*19*).

Acknowledgment

A.C.W. is indebted to the SERC for financial support during this investigation.

References

1. R. J. D. Tilley and A. C. Wright, *Chem. Scr.* **19,** 18 (1982).
2. R. J. D. Tilley and A. C. Wright, *Chem. Scr.* **19,** 68 (1982).
3. J. R. Gannon, R. J. D. Tilley, and A. C. Wright, *Mater. Res. Bull.* **16,** 1569 (1981).
4. M. Hansen and K. Anderko, "Constitution of Binary Alloys," 2nd ed., p. 1305, McGraw–Hill, New York (1958).
5. P. Bayliss and W. Nowacki, *Kristallografiya* **135,** 308 (1972).
6. V. Kupčik and L. Vesela-Novakova, *Tschermaks Mineral. Petrogr. Mitt.* **14,** 55 (1970).
7. S. Andersson and A. Åström, *in* "NBS Spec. Pub. 364, Solid State Chem." (R. S. Roth and S. J. Schneider, Eds.), NBS, Washington, D.C. (1972).

8. B. G. HYDE, S. ANDERSSON, M. BAKKER, C. M. PLUG, AND M. O'KEEFE, *Prog. Solid State Chem.* **12,** 273 (1979).
9. V. M. KOSEVICH, A. S. SOKOL, AND A. G. BAGMUT, *in* "Proceedings, 9th International Conference on Electron Microscopy, Toronto, Royal Microscopical Society," Vol. 1, p. 312 (1978).
10. J. C. PORTHEINE AND W. NOWACKI, *Z. Kristallogr.* **141,** 79 (1975).
11. J. R. CRAIG, L. L. Y. CHANG, AND W. R. LEES, *Canad. Mineral.* **12,** 199 (1973).
12. P. L. GARVIN, *Neues Jahrb. Mineral. Abh.* **118,** 235 (1973).
13. B. SALANCI AND G. MOH, *Neues Jahrb. Mineral. Abh.* **11,** 524 (1970).
14. B. SALANCI, *Neues Jahrb. Mineral. Abh.* **135,** 315 (1979).
15. A. G. NORD, Univ. Stockholm Inorg. Phys. Chem., D155, Vol. 33, p. 42 (1969).
16. P. E. WERNER, *Ark. Kemi* **31,** 513 (1969).
17. H. E. SWANSON, NBS circular 539, Vol. V (1955).
18. E. W. NUFFIELD, *Univ. Toronto Stud. Geol. Ser.* **50,** 49 (1946).
19. R. J. D. TILLEY AND A. C. WRIGHT, in preparation.
20. Y. U. TAKEUCHI, J. TAKAGI, AND T. YAMANAKA, *Z. Kristallogr.* **140,** 3/4, 9 (1974).